Full Paper

Israel Journal of Chemistry

DOI: 10.1002/ijch.201900073

# Fatty Acid Triangulation in Albumins Using a Landmark Spin Label

Jörg Reichenwallner,[a] Till Hauenschild,[a] Christian E. H. Schmelzer,[b, c] Miriam Hülsmann,[d] Adelheid Godt,[d] and Dariush Hinderberger*[a]

**Abstract:** Several spatial correlations of up to six fatty acid (FA) binding sites in albumins were found by double electron-electron resonance (DEER). A strategy was used that combines spin-labeling and spin-probing techniques in electron paramagnetic resonance (EPR) spectroscopy. This is here achieved by introducing an additional covalent landmark spin (LS) label to the self-assembled system of EPR-active, paramagnetic stearic acid derivatives and albumins. Therefore, a cysteine specific, paramagnetic LS that was attached to the albumin surface at a unique position (Cys34) provides a fixed topological reference point for monitoring statistical ligand uptake. We propose that the determination of nanoscale distance distributions emerging between the LS and EPR-active fatty acid derivatives generally allows for the direct observation of individually occupied binding sites in solution. Essentially, several binding pockets, groups of them and evidence for ligand-induced allosteric modulation can be traced from such FA-LS interspin correlations. Experimental results were substantiated with theoretical predictions from molecular dynamics (MD) simulations. It was observed that all binding sites in an albumin ensemble may be statistically filled even at the lowest level of ligand loading. This approach generally bears the potential for mapping occupation states of individual ligand binding sites in proteins using such spin-labeled ligands.

**Keywords:** DEER · EPR spectroscopy · Fatty acids · Albumin · Self-assembly

## 1. Introduction

In the last six decades, a multitude of impressive efforts have been undertaken to unravel the complex dynamic binding behavior of long chain fatty acids (LCFA) to albumins that constitute the major transport proteins in blood plasma of mammals.[1] The determination of individual binding affinities ($K_A$) of overall $N_T = 6–9$ major binding sites[2–4] is typically obtained upon application of multiple equilibria models, or related strategies for quantifying ligand binding properties of albumin.[5–7]

It has been proven that this binding site quantification in albumins is best achieved by utilizing equilibrium dialysis and partitioning methods,[2,6,8–11] $^{1}$H- and $^{13}$C-NMR spectroscopy,[12–17] 2D-NMR spectroscopy,[4,18] or spin probing strategies in continuous wave (CW) EPR spectroscopy that are based on non-covalent attachment of e. g. paramagnetic doxyl stearic acids (DSA) with the protein.[3,19–23] In terms of magnetic resonance methods, solution NMR spectroscopy has the advantage of screening for environmental inhomogeneities between individual binding sites,[24] whereas CW EPR spectroscopy is particularly suitable for screening binding site affinity ($K_A$) and ligand capacity ($N_T$) that can be obtained for virtually any paramagnetic, albumin-binding ligand.[25]

A major breakthrough in albumin research has been achieved with X-ray crystallography, revealing the distinct locations of individual fatty acid binding sites ($FA_i$). These binding sites were found to be distributed in an asymmetric arrangement within the crystalline state of human serum albumin (HSA).[26–28] They can be spatially correlated and separated into high ($FA_2$, $FA_4$ and $FA_5$) and low affinity ($FA_1$, $FA_3$, $FA_6$ and $FA_7$) binding sites.[29,30] However, a major drawback of X-ray crystallography is the inherent inaccessi-

[a] *J. Reichenwallner, T. Hauenschild, D. Hinderberger*
Institute of Chemistry, Martin Luther University Halle-Wittenberg, Von-Danckelmann-Platz 4, D-06120 Halle (Saale), Germany
phone: +49 (0)345 55-25130
fax: +49 (0)345 55-27576
E-mail: dariush.hinderberger@chemie.uni-halle.de
[b] *C. E. H. Schmelzer*
Fraunhofer Institute for Microstructure of Materials and Systems IMWS, Walter-Hülse-Straße 1, D-06120 Halle (Saale), Germany
[c] *C. E. H. Schmelzer*
Institute of Pharmacy, Martin Luther University Halle-Wittenberg, Wolfgang-Langenbeck-Straße 4, D-06120 Halle (Saale), Germany
[d] *M. Hülsmann, A. Godt*
Faculty of Chemistry and Center for Molecular Materials (CM2), Bielefeld University, Universitätsstraße 25, D-33615 Bielefeld, Germany

Supporting information for this article is available on the WWW under https://doi.org/10.1002/ijch.201900073

bility of the spatial FA arrangement in the functional solution structure of albumin.

In recent years we have devised an EPR spectroscopic research platform[31] that relies on the possibility to retrieve nanoscale distance information from albumin-bound DSA ligands in solution[32–34] by using the four-pulse DEER technique.[35,36] In standard experiments, this pulse EPR technique provides access to intramolecular distances from EPR-active biomolecules in the range of about 1.8–6.0 nm[37] at X-band frequencies (9.4 GHz). Despite its capability to determine these albumin-bound paramagnetic FA alignments, this approach still suffers from the arbitrary nature of mutual self-assembly of ligand and substrate. This is because one essentially obtains only the reduced, "negative" structural image as a kind of motion capture snapshot from the radical-bearing nitroxide groups in DSA when residing in the respective binding pockets. Entanglement of multiple and partially coincident nitroxide interspin distances between several bound DSA ligands typically obscures data analysis in terms of extracting individual $FA_i$ contributions. Yet, this problem can be partially overcome by correlating FA-derived interspin distances from DEER experiments to an appropriate crystal structure. For example, the construction of $(7 \times 7)$ distance matrices from HSA, co-crystallized with seven stearic acids[28] proved to be very promising in this regard.[32]

As mentioned above, such DEER data do not resolve individually occupied binding sites, nevertheless, they allow for drawing some conclusions about the plasticity of the protein surface and interior. Remarkably, it was found that the DEER-derived distribution from 16-DSA spin probes representing HSA's surface does not coincide with the crystal structure-derived data, whereas 5-DSA confirms the aforementioned picture of an asymmetric protein interior.[32] In this context the number in Y-DSA represents the chain position of the nitroxide reporter group in relation to the carboxyl group of stearic acids (CY=C1 atom). This circumstance provides a case-specific inside-outside perspective on the protein as FAs mostly bind with their carboxyl to an ionic anchor inside albumin.[28] Furthermore, unlike in bovine serum albumin (BSA), the FA distribution in HSA does not significantly change with the FA loading status.[32,33] In fact, the DEER-derived FA alignment on BSA's surface resembles HSA's crystal structure-derived data quite well, especially for higher loadings. For now, these findings remain largely unexplained in terms of individual $FA_i$ contributions, although differences in amino acid hydropathies in the corresponding tertiary structures could be identified as one of the major causes that alter internal albumin dynamics and ligand alignments likewise.[38] Basically, these analytical assignment problems consistently emerge due to the inherent lack of spatial reference points in DEER experiments on albumins as a consequence of the statistical binding processes of FAs.[12]

To achieve further insights into the binding process of individual FA and to identify each binding site in EPR spectroscopic data ($FA_i$), a hybrid strategy is here employed that combines spin-probing and spin-labeling, i.e. non-covalent and covalent attachment of EPR-active reporter groups, respectively (see also Figure 1). Nowadays, it is however not uncommon in EPR spectroscopy to determine such label-to-probe distances.[39–42]

Generally, this study was inspired by the earliest spin-labeling experiments on albumin with the 3-amino-proxyl,[43]

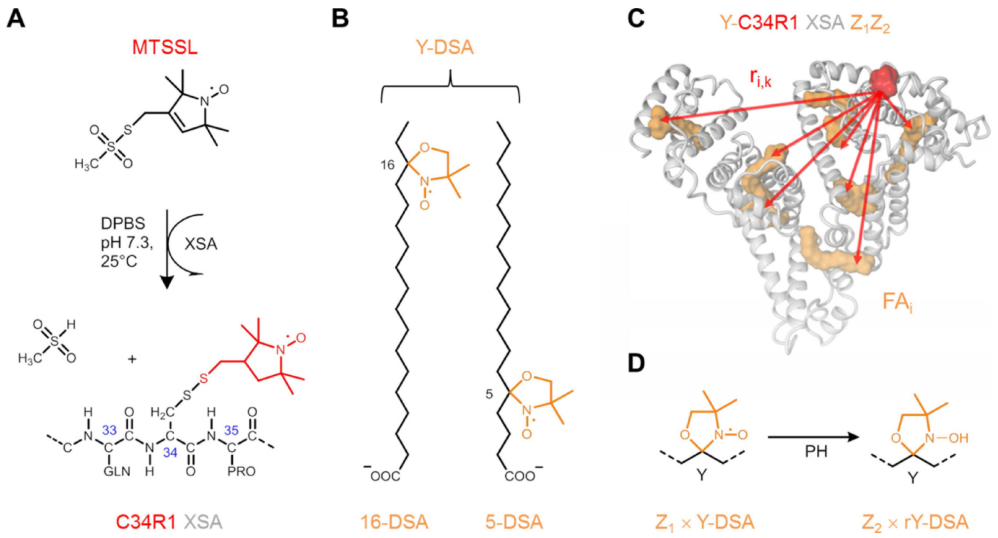


**Figure 1.** Introduction of a located landmark spin (LS) label to albumin for FA triangulation in a combined approach using spin-labeling and spin-probing. (A) Covalent attachment of cysteine selective MTSSL to the Cys34 residue[55] of XSA leading to C34R1 XSA.[46,48] (B) Chemical structure of the spin probes 5-DSA and 16-DSA with the doxyl groups highlighted in orange. (C) Molecular model constructed (from PDB ID: 1e7i)[28] that facilitates tracking of individual distances ($r_{i,k}$) to a maximum of seven ($Z_1Z_2 = 70$, or 16) aligned spin probes (orange) with the LS. (D) Schematic representation of Y-DSA reduction with phenylhydrazine (PH) to EPR-silent rY-DSA ligands that can be added to C34R1 XSA in appropriate loading ratios $Z_1$ and $Z_2$.

or 3-maleimido-proxyl spin labels.[44] However, these reagents typically generate a mixture of lysine- and cysteine-labeled albumins resulting in the emergence of rather unspecific labeling sites.[44,45] Selective labeling of the highly conserved Cys34 residue[1] in HSA with the cysteine-specific methanethiosulfonate spin label (MTSSL) was reported earlier,[46,47] serving as a tool for investigations on e. g. albumin fragment dynamics.[46] Recently, this approach was also adopted in DEER spectroscopy for proving interactions of HSA with the copper transporter Ctr1[48] and for investigating surface adhesion and dimerization effects of BSA with the latter one being equipped with the cysteine specific iodoacetamide (IAA) spin label.[49]

Here, we covalently attach MTSSL to obtain such a C34R1 albumin variant that we then employ for monitoring FA binding events from a remote, binding site-independent, topological position in both, HSA and BSA. This strategic ligand triangulation position (C34R1) is thus regarded as a protein-based topological landmark site for ligand entry. The crystal structures of both albumin apoproteins[50,51] were found to be largely congruent.[38] Therefore we can assume that the binding pockets, in particular the interior cationic head-end to which the anionic carboxylic acid of the FAs can bind (C1 position), are located at similar positions in both proteins.

Here, we expand our EPR spectroscopic albumin research platform,[31] by simultaneously triangulating positions of protein-bound FAs through incorporation of a landmark spin (LS = C34R1) to the system. We aim at identifying distinct $FA_i$ locations in the solution state of HSA and BSA by analyzing such DEER-derived (LS-$FA_i$) distance distributions. In addition, we use MD simulations starting from the crystal structure of HSA containing seven stearic acids (PDB ID: 1e7i)[28] and include the results from literature to analyze our EPR-based distance data. While proving whether the binding sites are filled consecutively or arbitrarily, we also contribute new aspects about how the dynamic complexity of FA binding to albumin can be further unraveled in the solution state.

## 2. Results and Discussion

### 2.1 Spin-Labeling of Albumins

In our hybrid spin-probing and spin-labeling strategy, HSA and BSA were equipped with MTSSL to yield a spatially fixed landmark spin label at the native accessible Cys34 residue (LS = C34R1, Figure 1A). These spin-labeled albumins (X) are furthermore denoted as C34R1 XSA. The application of dithiothreitol (DTT) as a sulfhydryl reducing agent during the labeling procedure was discouraged, as even low amounts of DTT (about 1–10 eq) had a negative effect on ligand affinity. Alternatively, the free sulfhydryl contents of pure albumin and spin-labeled albumin solutions were determined with the standard Ellman's test[52] prior to labeling. These sulfhydryl concentration values were then used together with the quantitative bicinchoninic acid (BCA) assay[53] to determine the labeling efficiency and protein content similar to Berliner et al.[54] This was done in order to load each protein with appropriate and comparable amounts of paramagnetic 5-DSA and 16-DSA for conducting the fatty acid triangulation in albumin (Figure 1B and 1C). MALDI-TOF mass spectrometry on the spin-labeled albumins revealed relative molecular weight (MW) increases of about $\Delta MW = 187 \pm 9$ Da for HSA and BSA as it can be theoretically expected ($\Delta MW_{R1} = +184.28$ Da, Table 1). A further confirmation of spin-labeling was obtained with CW EPR spectroscopy (Figure 2A) showing spectra that resemble the line shapes reported in Park et al.[46] quite well. The broad spectral lines are indicative of strongly immobilized MTSSL being covalently attached to any albumin (XSA). It could be shown by spectral simulation that C34R1 XSA typically contains less than about $\varphi_f = 0.5\%$ of unbound MTSSL (free = $f$) after purification. Albumin-bound MTSSL exhibits several dynamic regimes with strong and weak immobilization (bound = $b_i$) that may differ in relative occupation for HSA and BSA. A second moment analysis on these CW EPR spectra indicates that the LS is structurally more buried on the C34R1 HSA surface in comparison to C34R1 BSA (Figure S13D). The results from the C34R1 XSA characterization are summarized in Table 1.

It is commonly accepted that the thiol content in albumin samples exhibits a certain heterogeneity[56] that mainly depends on individual physiological conditions.[57] Usually, an antiox-

**Table 1.** Characterization of C34R1 XSA samples.

| Sample | $c_{BCA}$[a] [mM] | $c_{SH}$ [mM][b] | $\varphi_{SH}$[c] [%] | MW[d] [Da] | $\varphi_f$[e] [%] |
|---|---|---|---|---|---|
| 1 mM BSA | 0.936 ± 0.098[f] | 0.511 | 54.6 | 66446 | – |
| 1 mM HSA | 0.818 ± 0.044[f] | 0.243 | 29.7 | 66531 | – |
| C34R1 BSA | 0.422 ± 0.025 | – | – | 66642 | < 0.5 |
| C34R1 HSA | 1.000 ± 0.090 | – | – | 66709 | < 0.3 |

[a]All protein concentration values ($c_{BCA}$) were determined with BCA assays.[53] [b]Free sulfhydryl content ($c_{SH}$) was determined with Ellman's tests.[52] [c]$\varphi_{SH} = c_{SH}/c_{BCA}$ is the fraction of accessible thiols per albumin = observed labeling effciency. [d]Molecular weights (MW) were determined with MALDI-TOF (see Figures S3–S6). [e]Fraction of unbound MTSSL molecules ($\varphi f$) from the purified stock solutions is given in area percent of the full EPR spectrum. [f]Concentrations deviate from the nominal value of 1 mM due to excluded volume effects.[5]

Israel Journal of Chemistry

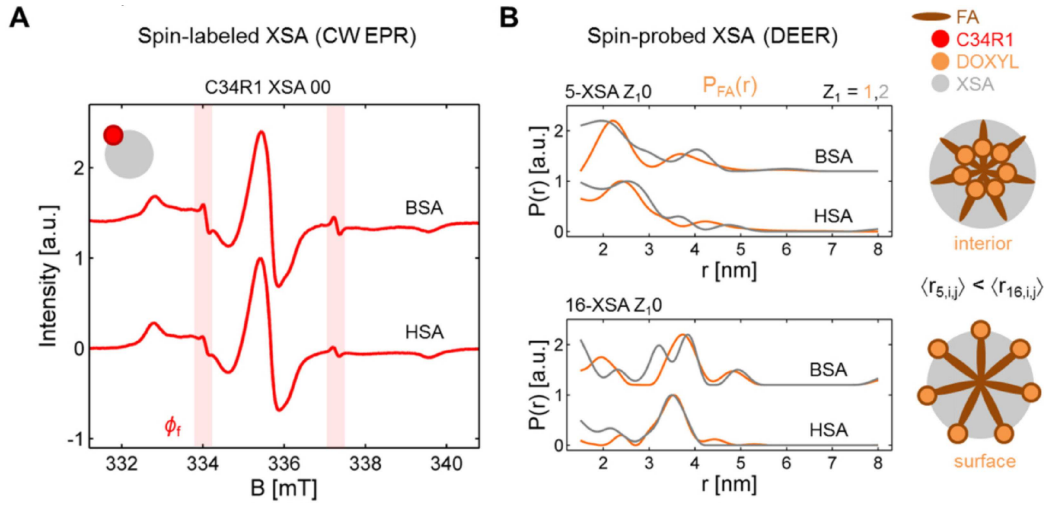


**Figure 2.** Spin-labeled and spin-probed albumins. For simplicity, albumins are additionally given in sketches represented in gray (XSA), with C34R1 in red, doxyl groups in orange spheres and FA chains are given as brown rods. (A) CW EPR spectra are shown from the pure spin-labeled proteins C34R1 XSA 00 at $c = 0.62$ mM. The residual unreacted MTSSL ($\varphi f$) is exemplary highlighted for HSA and BSA with red bars. (B) DEER experiments on Y-DSA-probed XSA (Y-XSA $Z_1 0$) at $c_H = 0.336$ mM and $c_B = 0.183$ mM (pH 7.4 in DPBS buffer and 20% v/v glycerol). Albumin-bound FA distributions $P_{FA}(r)$ emerge from XSA loaded with one (orange) or two (gray) paramagnetic FA equivalents ($Z_1$ is 1 or 2). DEER data were processed in DeerAnalysis and validated distributions are given in Figure S17B.[67] The sketches given on the right hand side highlight that 5-DSA rather monitors the protein interior and 16-DSA the protein surface.[32] Accordingly, the mean interspin distances $\langle r_{Y,i,j} \rangle$ as observed from the paramagnetic doxyl groups are therefore generally shorter for 5-XSA.

idant role is ascribed to the conserved Cys34 residue in albumins.[58–60] Unexpectedly, the herein determined fraction of accessible thiols in HSA samples is quite low (~30%), while in previous literature it was suggested that 70–80% of the thiols exist in the reduced form in healthy individuals.[58,61] For BSA, various values are reported ranging from 36–69%[62] and, in contrast to HSA, these reference values coincide quite well with the findings made here (~55%).

There was no evidence of a yellow color stain in Ellman's tests from spin-labeled albumin solutions, adding another proof to the presence of labeled protein. Due to the many adjustable experimental parameters, distinctive sample identification was achieved as described in the following paragraph.

We here use an extensive sample identifier of the form: Y-C34R1 XSA $Z_1Z_2$, in which Y denotes the label position (C5 or C16 carbon) in Y-DSA, C34R1 denotes whether the investigated albumin species XSA was spin-labeled and $Z_1Z_2$ indicates the FA loading status of a sample. Here, $Z_1$ indicates the number of paramagnetic (Y-DSA) and $Z_2$ the number of reduced and diamagnetic FA equivalents (rY-DSA) that are here used for spin dilution (see Figure 1D).[32] Thus, e.g. 5-C34R1 HSA 16 is a spin-labeled HSA sample that is probed with one paramagnetic and six diamagnetic 5-DSA probes and 5-HSA 10 is a native (unlabeled) HSA protein containing only one EPR-active 5-DSA probe.

A set of reference DEER experiments of XSA loaded with Y-DSA is shown in Figure 2B that were presented similarly in earlier studies.[32,38] In this graph the typical FA-based, coarse-grained view of the albumin interior (Y = 5) and surface (Y = 16) is observed (see also the simplified sketch on the right hand side). Spin-probed 5-HSA shows the typical peaks at about 2.3–2.5 nm and 3.5 nm for 16-HSA. From spin-probed 5-BSA we again find the characteristic peaks at 2.0–2.2 nm and 3.2 nm, as well as 3.8 nm for 16-BSA. However, the peak at 3.2 nm only emerges for higher loadings (16-BSA 20). Slight variations in distribution shape can be observed when compared to earlier published data. The qualitative outcome remains the same.

According to the different labeling efficiencies $\varphi_{SH}$ of HSA and BSA (Table 1) the R1 concentration in each sample was adjusted to be constant at 0.1 mM to certify sufficient signal strength for all EPR-based distance measurements. Moreover, a 0.1 mM equivalent of R1 corresponds to $c_H = 0.336$ mM HSA and $c_B = 0.183$ mM BSA. Double integration (DI) of corresponding CW EPR spectra of spin-labeled but spin probe-free samples (C34R1 XSA 00) confirmed the validity of this approach. In the next section we will combine these two separate EPR-active systems from Figure 2 experimentally.

### 2.2 DEER Experiments on Spin-Probed C34R1 Albumins Containing a Landmark Spin

As the C34R1 residue is spatially fixed, it is now defined as a protein-based topological landmark for all additional spins that are introduced upon addition of EPR-active FAs (Y-DSA). Therefore, a systematic variation in FA content is expected to allow for characterizing the binding sequence and binding site occupation from changes in DEER-derived distance distributions. In Figure 3 all experimental DEER time traces are

  

Israel Journal of Chemistry

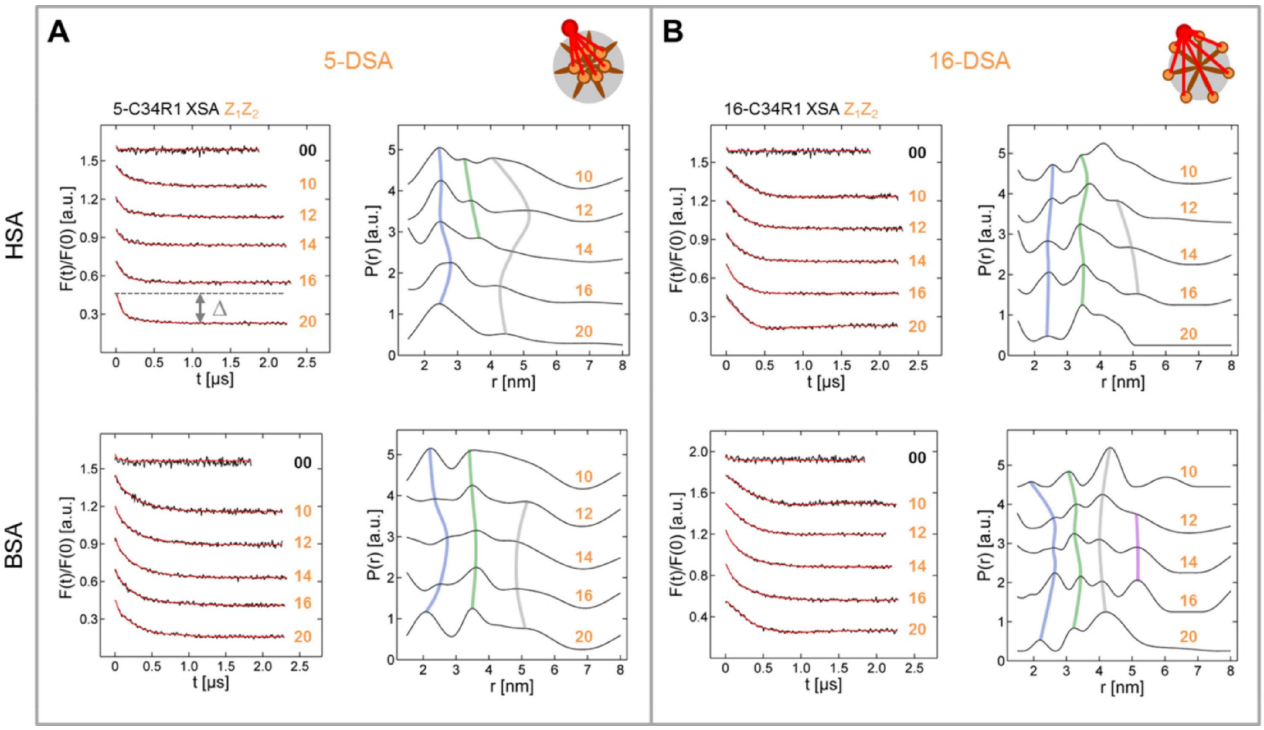


**Figure 3.** DEER time traces of spin-probed albumins bearing a landmark spin. This collection of dipolar evolution functions $F(t)/F(0)$ and corresponding regularized fit curves (red) shows (A) 5-C34R1 XSA $Z_1Z_2$ and (B) 16-C34R1 XSA $Z_1Z_2$ together with their respective distance distributions $P(r)$ as obtained from DeerAnalysis.[67] Validated distributions are given in Figures S18 and S19. Samples were equipped with paramagnetic ($Z_1$) to reduced ($Z_2$) FA ratios of 0:0, 1:2, 1:4, 1:6 and 0:0 (orange identifiers). Additionally, a FA-free sample (0:0, black identifier) is shown for both albumins in order to highlight the presence of dipolar modulation in all other DEER time traces. The modulation depth Δ is indicated for 5-C34R1 HSA 20 in gray. Several recurrent features are tracked with blue, green, gray and purple lines in $P(r)$ graphs. The simplified scheme of the investigated spin triangulation system is given according to Figure 2 at the top right side of each box.

shown that were obtained from Y-C34R1 XSA $Z_1Z_2$ samples equipped with $Z_1$ paramagnetic and $Z_2$ diamagnetic FAs. It should be mentioned here, that upon using the topologically fixed LS, only one equivalent of paramagnetic and an increasing number of reduced FAs ($Z_2 = 2$, 4 and 6 equivalents of rY-DSA) were added to both spin-labeled albumins to emulate spin-diluted ligand loading. The data sets are complemented through samples with a 0:0 loading (lower traces) to highlight the effect of a relative excess of paramagnetic FA. Typically, the number of coupled spins is thus kept below $\langle n \rangle = 2$ to prevent peak distortions in $P(r)$ by multispin artifacts.[32,33,63]

The upper trace in Figure 3 shows C34R1 XSA 00 albumins as a reference, resembling a *monoradical* protein that exhibits largely modulation free time traces ($\Delta < 0.08$), i.e. experimental data lacking dipolar modulation (see also Figure S17A). The background dimensionalities are about $D = 3$ and therefore the number of coupled spins is close to one ($\langle n \rangle = 1.05$–$1.16$, see equation 3). This is also indicative for the absence of a strong dimerization propensity of albumins in solution at the experimental conditions of choice, especially for pH.[49] A clear increase in signal-to-noise-ratio (SNR) and modulation depth Δ is observable upon loading Y-DSA and rY-DSA on spin-labeled albumin. CW EPR-based spin counting routines of spin-diluted samples are intrinsically hampered and hence all recorded CW EPR spectra look quite similar (Figure S9). Although the dipolar evolution functions in DEER experiments on Y-C34R1 XSA $Z_1Z_2$ samples also exhibit similar Δ values (see also Figure S16) it is again indicative of a successful reduction procedure (Y-DSA to rY-DSA, Figure 1D).

For more reliable spin counting procedures we here used monodisperse oligo-*para*-phenylene ethynylene (oligoPPE) dinitroxides as a reference substance ($\langle n \rangle = 2$ electron spins per molecule). In these molecules two nitroxide moieties are bound via a rod-shaped rigid PPE spacer with adjustable length.[64] The distance distributions of these dinitroxides are well-known[65,66] and the device-specific modulation depth parameter ($\lambda = 0.534$) could be determined that is essential for spin counting procedures.[63,67–70] Here, the application of oligoPPE dinitroxides of varying length (from 2.8–7.5 nm, see Figure S15) proves $\lambda$ to be distance-independent as well.

Thus, this value could then be used to calculate and estimate the average number of coupled spins $\langle n \rangle_X$ from all FA-loaded samples, giving $\langle n \rangle_H = 1.39 \pm 0.10$ for spin-probed C34R1 HSA and $\langle n \rangle_B = 1.69 \pm 0.09$ for spin-probed C34R1 BSA (see Figure 4A). In turn, this finding corresponds well with our data obtained from Ellman's tests (i.e. $\varphi_{SH} \approx \langle n \rangle_X - 1$,

  

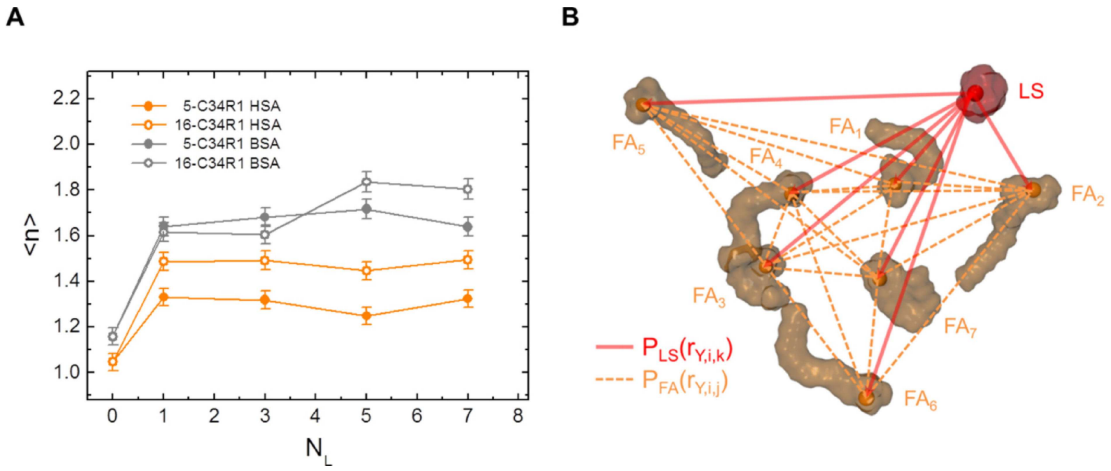


**Figure 4.** Spin counting and distance correlations in Y-C34R1 XSA $Z_1Z_2$. (A) Results from spin counting where the number of coupled spins $\langle n \rangle$ is higher for Y-MTSSL BSA due to the higher labeling efficiency $\varphi_{SH,X}$. $\langle n \rangle$ also remains largely constant throughout ligand loading ($N_L = Z_1 + Z_2$) due to the applied spin dilution strategy. (B) The molecular model of 16-C34R1 HSA 70 was constructed in YASARA Structure[83] from PDB ID: 1e7i[28] and is used for generally highlighting the nitroxide positions of 16-DSA (orange balls) and the landmark spin (LS, red ball) as they are observed in DEER experiments. All individual fatty acid binding sites ($FA_i$) are presented according to their alignment in the protein scaffolding (suppressed) and their interspin distances $r_{Y,i,j}$ (orange dotted lines) that lead to the established *standard interspin system* $P_{FA}(r)$.[32] The introduction of a LS (red) leads to the emergence of additional distances $r_{Y,i,k}$ (red lines) defining the *reduced interspin system* $P_{LS}(r)$.

see also Table 1) and is additional evidence that the accessible thiols have reacted with MTSSL to a large extent.

All distance distributions $P(r)$ that are shown in Figure 3 were derived from corresponding dipolar evolution functions in the time domain. Processing DEER time traces in DeerAnalysis[67] was conducted in a consistent scheme throughout, assuming an excluded volume-induced background dimensionality of $D = 3.74 \pm 0.03$.[32,71] Nevertheless, the general shapes of individual probability densities $P(r)$ remain intricate and were therefore validated (Figures S18 and S19).

In a global view several features can be identified as indicated with the blue, green, gray and purple lines that prove the validity of most distance distributions by characteristic peaks at almost identical positions (see 5-C34R1 BSA (green line), or 16-C34R1 HSA (blue line)). Furthermore, no distance probability density should be observable in the range of the hydrodynamic diameter of albumin ($R_H \sim 6.2$–$7.0$ nm).[72]

Several distance features change upon FA loading and we assume that this effect emerges due to the increased binding site occupation and a simultaneous allosteric modulation of the albumin proteins during FA binding.[73] For now, the ascribed significances in $P(r)$ are to be handled with care due to the limitations emerging from short dipolar evolution functions (up to ~5.2 nm).[37] All peak characteristics beyond 4.5–5.0 nm are either blurred (see also data validation in Figures S18 and S19), or may emerge due to background artifacts and cannot be distinctively interpreted.[67]

Note that the distance distributions in Figure 3 clearly differ from purely spin-probed XSA (Figure 2B) and it is now safe to assume that the statistical distribution of fatty acids in XSA leads to an overlap of LS-$FA_i$ distances and $FA_i$-$FA_j$-distances. Thus, even if only one equivalent of EPR-active FAs is used, there may always be a fraction of individual albumin molecules that have two DSAs loaded.[12,14] Hence, a more elaborate approach had to be chosen for a better FA assignment.

### 2.3 Rationalizing Distance Distributions from Spin-Probed C34R1 Albumins

To enable distance peak assignments, two molecular models were constructed from the crystal structure of HSA co-crystallized with stearic acids (PDB ID: 1e7i)[28] with a R1 residue at backbone position Cys34 either loaded with seven 5-DSA, or seven 16-DSA ligands. With these models, MD simulations were performed (see Supporting Information S2). This approach is primarily based on the scheme applied in Junk et al.[32] that allows for extracting a set of theoretical $FA_i$-$FA_j$-distances. This expanded approach here thus bears the potential of simultaneously tracking theoretical distances between the LS and individual FAs, as well as the $FA_i$-$FA_j$-distances.

One primarily expects to obtain seven distinct LS-$FA_i$ distances ($r_{Y,i,k}$) corresponding to the respective binding pockets ($P_{LS}(r)$), i.e. the individual paramagnetic center in it. The complete set of $N_{r,FA} = (N_{FA}^2 - N_{FA})/2 = 21$ fatty acid-only interspin distances ($FA_i$-$FA_j$) that are aligned in albumin are given in the $7 \times 7$ matrix of the *standard interspin system* ($P_{FA}(r)$, see Figure 2B).[32] Indeed, by introducing the LS, the *extended interspin system* $P(r)$ spans an $8 \times 8$ matrix and has $N_{LS} = 7$ theoretical distances more with a total of $N_{r,LS} = 28$ interspin distances (see Figure 4B and Tables S3–S5). A full

theoretical distribution $P_{MD}(r_{Y,i,j,k})$ with all spin correlations for Y-C34R1 XSA 70 is constructed from such a 8×8 distance matrix according to the relation:

$$P_{MD}(r_{Y,i,j,k}) = \frac{1}{|A|} \cdot \sum_{i \neq j \neq k}^{N_{r,Y,LS}} \exp\left(-\frac{(r - r_{Y,i,j,k})}{2\sigma}\right)^2 \quad (1)$$

where $|A|$ is a normalization constant and $\sigma$ is the width of the artificial Gaussian broadening.

The first step is now to analyze $P_{LS}(r)$ from MD simulations yielding a list of probe-specific LS-FA$_i$ distances ($r_{Y,i,k}$, red) as presented in Table 2. For clarity, the well-known corresponding subdomains of the FA binding sites are also given.[28,74] Individual distance values are taken as an average from 10–15 simulation snapshots of according trajectories in Figure S11 for $t_{MD} > 5$ ns. This strategy is here considered as largely sufficient because the standard deviations of individual LS-FA$_i$ distance values from MD simulations are generally found to be quite small ($\Delta r_{Y,i,k} \leq 0.27$ nm).

In principle, all paramagnetic centers of the modeled FAs can be considered to range within appropriately remote distances relative to the LS. These distances are either smaller, or similar compared to the simulation-derived gyration diameter $2R_G = 5.74$ nm of albumin (Figure S11). This is in good agreement with results from small-angle neutron scattering (SANS) experiments ($2R_G = 5.48$ nm).[75]

First systematic restrictions emerge from values shown in Table 2. In 16-C34R1 XSA, $FA_2$ ($r_{16,2,k} \sim 1.5$ nm) and $FA_5$ ($r_{16,5,k} \sim 6.1$ nm) have to be considered as being experimentally inaccessible due to the aforementioned limited time trace resolution ($t_{max} \leq 2.5$ µs) and proton modulation. Furthermore, in 5-C34R1 XSA, several LS-FA$_i$ distances ($FA_{3\text{-}6}$) are so similar that they should be indistinguishable in DEER experiments. The same holds true for fatty acid pairs $FA_3$, $FA_6$ that are about 5 nm and $FA_4$, $FA_7$ that are about 3.6 nm away from the LS in 16-C34R1 XSA. However, some distances are unique in this reduced interspin system $P_{LS}(r)$ and should be clearly identifiable in $P(r)$. In principle all values in Table 2 are absolute values of distance vectors that are generally defined by length and (relative) orientation.

**Table 2.** LS-FA$_i$ distances $r_{Y,i,k}$ from MD simulations in $P_{LS}(r)$.

| LS = k<br>FA$_i$ | 5-DSA<br>$r_{5,i,k}$[a] [nm] | 16-DSA<br>$r_{16,i,k}$[b] [nm] | FA$_i$ location<br>Subdomain[c] |
|---|---|---|---|
| 1 | 2.48 ± 0.10 | 2.65 ± 0.11 | IB |
| 2 | 3.25 ± 0.08 | 1.49 ± 0.19 | IB |
| 3 | 5.26 ± 0.15 | 5.11 ± 0.13 | IIIA |
| 4 | 5.03 ± 0.14 | 3.69 ± 0.16 | IIIA |
| 5 | 5.43 ± 0.27 | 6.06 ± 0.17 | IIIB |
| 6 | 5.22 ± 0.14 | 4.86 ± 0.09 | IIA-IIB |
| 7 | 3.77 ± 0.10 | 3.62 ± 0.13 | IIA |

[a]Averaged distance values $r_{5,i,k}$ in the range from 6.5 ns < $t_{MD}$ < 21.3 ns simulation runtime from Figure S11A. [b]Averaged distance values $r_{16,i,k}$ in the range from 5.8 ns < $t_{MD}$ < 27.1 ns simulation runtime from Figure S11B. [c]Domain assignment of FA$_i$ binding site location is given according to Bhattacharya et al.[28] and Ghuman et al.[74]

With albumin we investigate a highly flexible and adaptable structural scaffolding. Intrinsically, individual distances $r_{Y,i,j,k}$ that were extracted from MD simulations implicitly contain relative angular information. Thus, angular correlations were not investigated in depth. Sophisticated experimental setups and analytic procedures are for now not required.[76–79] A further obstacle for such data analyses is that individual distance peaks in $P(r)$ may vary in relative intensities and positions upon FA loading due to the aforementioned general configurational adaptability, i.e. the emergence of allosteric modulation. This phenomenon is also known as the major functional aspect of albumin – structural plasticity – that was initially observed by Karush to affect ligand binding site cooperativity.[80,81] Particularly, a recent study proved that EPR spectroscopy is capable to elucidate the intrinsic entanglement of such intricate structural and dynamic properties when albumin is exposed to post-translational modifications (PTMs). Utilizing the DSA-probed BSA model system, it could be shown how specific PTMs may exert strong alterations on albumin-ligand interactions ($N_T$, $K_A$) that are again mirrored in corresponding ligand alignments and altered binding site occupations ($P(r)$), respectively.[82]

For highlighting the direct effect of the LS on $P(r)$, the FA-based distance distributions $P_{FA}(r)$ from Figure 2B and some key distance distributions of Y-C34R1 XSA (1 : 0, 2 : 0 and 1 : 6) from Figure 3 are compared in Figure 5.

Additionally, data from fully occupied Y-C34R1 XSA 16 samples are compared to theoretical distributions ($Z_1Z_2 = 70$) from exemplary simulation snapshots at 9.4 ns runtime (Table S5). This can be considered as the key step for binding site tracking in the present study.

In Figure 5A, the 5-C34R1 HSA system shows clear deviations from the pure FA-based distributions at lowest 5-DSA loadings ($Z_1Z_2 = 10$, gray, upper trace). There are three distinct peaks that can be exclusively assigned to LS-FA$_i$ distances at 2.48 nm ($FA_1$), 3.18 nm ($FA_2$), 4.08 nm ($FA_7$) and a broad, continuous part between about 4.5 and 6.0 nm that would correspond to all four spare distance vectors ($FA_{3\text{-}6}$). In Figure 5B, the 5-C34R1 BSA system shows a very similar distribution apart from the lack of the 3.2 nm feature ($FA_2$). It is therefore assumed that $FA_2$ and $FA_7$ distances coincide in BSA (2,7) and $FA_{3\text{-}6}$ also form the broad continuous part in the range from 4.5–6.0 nm. Unlike in HSA, the combined distance peak of $FA_2$ and $FA_7$ (2,7) in 5-C34R1 BSA persists throughout all loading ratios. These features are for now considered to clearly emerge from the LS and in a comparative view of HSA and BSA it is moreover indicative of how the labeling efficiency influences $P(r)$.

The distribution shape in 5-C34R1 HSA approaches the standard interspin system ($P_{FA}(r)$) distribution with higher loadings (FA, gray arrow), while 5-C34R1 BSA is still dominated by the reduced interspin system characteristics ($P_{LS}(r)$), mainly exhibiting LS-FA$_i$ distances (green arrow).

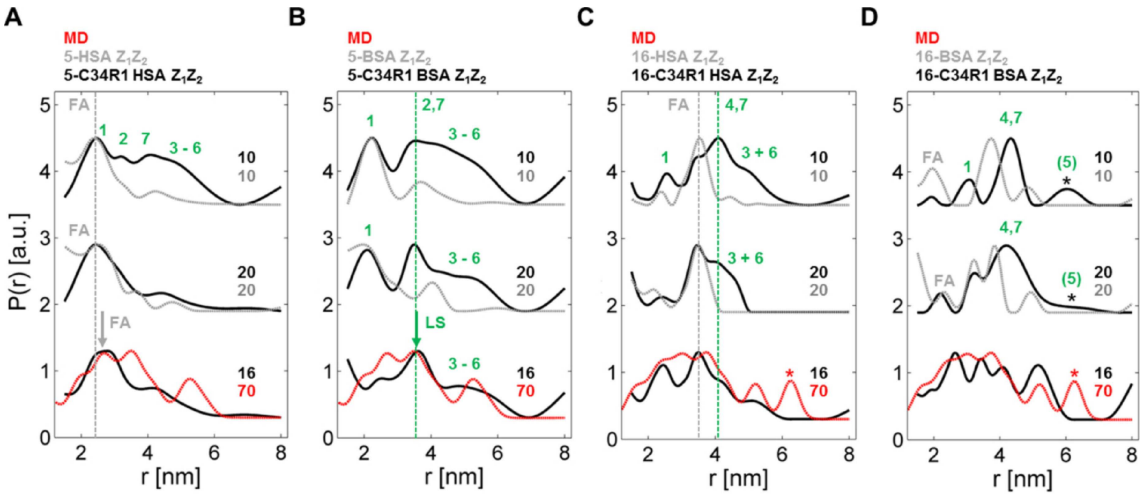


**Figure 5.** Rationalization of distance peaks in key distance distributions of spin-probed Y-C34R1 XSA $Z_1Z_2$. A comparison is shown between C34R1 XSA samples (black) and unmodified Y-XSA samples from Figure 2B lacking the LS (gray) for (A) 5-C34R1 HSA, (B) 5-C34R1 BSA, (C) 16-C34R1 HSA and (D) 16-C34R1 BSA (*=black, implications for $FA_5$). Both albumins were either loaded with one ($Z_1Z_2=10$, upper traces) or two ($Z_1Z_2=20$, middle traces) equivalents of 5-DSA or 16-DSA. Theoretical distributions $P_{MD}(r_{Y,i,j,k})$ ($Z_1Z_2=70$, $\sigma=0.17$, red (MD)) were aligned with the fully occupied Y-C34R1 XSA 16 samples (lower traces) from snapshots at $t_{MD}=9.4$ ns (Table S5, red, *=allegedly inaccessible in DEER experiments conducted here). Resemblances with FA-induced distribution shapes are denoted as "FA" (gray) and conformity with values in Table 2 are denoted with corresponding $FA_i$ identifiers ($i=1$–7, green) from the reduced interspin system $P_{LS}(r)$). When applicable, recurrent characteristics are aligned with dotted lines or arrows in according colors.

This characteristic difference is also reflected in the theoretical MD-derived distance distribution (70, red), where each distance value $r_{Y,i,j,k}$ of the $8\times8$ matrix is represented with identical weight (see equation 1). The major finding at this point is that even at the lowest 5-DSA loadings (5-C34R1 XSA 10) an almost complete set of $FA_i$ assignments can be devised. This proves that at the near physiological albumin concentrations used here, the binding sites are not filled consecutively, i.e. according to their individual strength ($K_{A,i}$), but randomly in the albumin ensemble ($K_A \approx 10^6$–$10^8\ M^{-1}$, nM to µM regime).[3,21] Thus, all individual binding site affinities ($K_A$,$i$) appear to be more or less equivalent, or at least in a similar order of magnitude when a single FA loading equivalent is present.

As described above, $FA_2$ and $FA_5$ distances from bound 16-DSA in $P_{LS}(r)$ are assumed to be experimentally inaccessible with DEER. This is well confirmed for $FA_5$ by comparing theoretical distributions with experiments (Figures 5C and 5D, red asterisk, lower traces) as the feature around 6.2 nm in the red dotted line does not appear in the experimental distance distributions. Data from the 16-C34R1 HSA system in Figure 5C again shows clear deviations from $P_{FA}(r)$ at lowest 16-DSA loading (10, gray, upper trace). Here, four peaks emerge that can be assigned to $FA_1$ (2.55 nm), a combination of $FA_4$ and $FA_7$ at 4.09 nm (green dotted line), as well as a broad feature that is here ascribed to $FA_3$ and $FA_6$. Obviously, when compared to higher ligand loadings, the feature at 3.5 nm is identified to be again mainly generated by $P_{FA}(r)$ (gray dotted line) and unfortunately represents at least six identical interspin correlation distances ($FA_i$-$FA_j$) of individual 16-DSAs bound to HSA (see Tables S3–S5).

In contrast, the 16-C34R1 BSA system in Figure 5D shows a different distribution, resembling the combined and unique (4,7) feature at about 4.33 nm that can be also observed in 16-C34R1 HSA. The peak at 3.09 nm is only explicable when assigned to $FA_1$ and the small bump at about 2.1 nm that is visible in 2:0 and 1:0 loadings (Figure 2B), is again most probably induced by $P_{FA}(r)$, or it is an artifact. The asterisk (*) in Figure 5D (see 10 and 20 loading) appears to be a real distance component. According to data validation results this feature would represent $FA_5$. However, we refrain to put too much attention into this peculiarity as it is very weak. The distribution for 16-C34R1 BSA 20 features the typical 3.2 nm peak in purely FA-probed BSA. Unfortunately, the distance peaks for $FA_1$ in $P_{LS}(r)$ of 5-C34R1 HSA and 5-C34R1 BSA coincide with $P_{FA}(r)$ and are also found to be not clearly distinguishable. The general nature of the DEER-derived distance distributions from C34R1 XSA is therefore assumed to represent an (extended) mixture distribution $P(r)$ composed of $P_{LS}(r)$ and $P_{FA}(r)$ (Figures 6A and 6B). Mathematically, this mixture distribution can be described by the relation:[84,85]

$$P(r) = \sum_{m}^{N} f_m \cdot P_m(r) \qquad (2)$$

with $\Sigma f_m = 1$. The parameter $m$ defines the origin (LS-$FA_i$ or $FA_i$-$FA_j$) of the respective distance probability density being in consideration. The relative weight $f_m$ is assumed to strongly

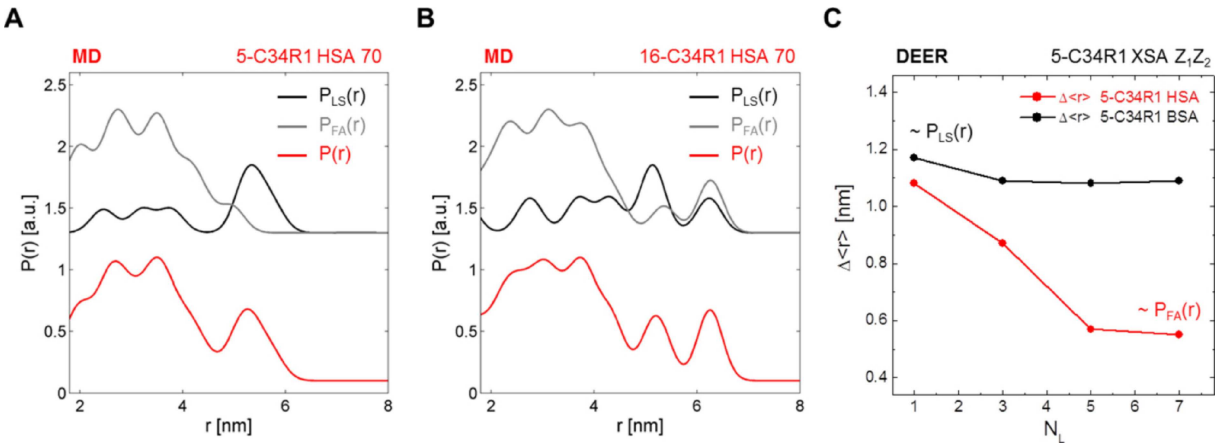


**Figure 6.** Theoretical mixture distributions and mixture distribution influence on experimental data. A mixture distribution $P(r) = P_{MD}(r_{Y,i,j,k})$ can be rationalized from molecular models of Y-C34R1 HSA 70 with the superposition of a reduced interspin system fraction $f_{LS}$ and a standard FA-based fraction $f_{FA}$. Therefore, $P_{LS}(r)$ (black) and $P_{FA}(r)$ (gray) are combined to yield $P(r)$ (red) for (A) 5-DSA and (B) 16-DSA aligned in C34R1 HSA 70. Data are taken from simulation snapshots at 9.4 ns in Table S5 with $\sigma = 0.17$. The relative weights were here set to $f_{LS} = 0.36 \approx \langle n \rangle_H - 1$ and $f_{FA} = 0.64 \approx 2 - \langle n \rangle_H$ for visualizing the individual contributions to $P(r)$. (C) The experimental difference in first moments,[86] or mean distances $\Delta\langle r \rangle = \langle r \rangle - \langle r \rangle_{FA}$ between $P(r)$ of 5-C34R1 XSA loading experiments is shown as derived from Figure 3A. This is due to the increased FA-based influence on $P(r)$ when the labeling efficiency $\varphi_{SH}$ varies in between different albumin species.

depend on labeling efficiency (see Table 1 ($\varphi_{SH} \approx \langle n \rangle_X - 1$)), the relative affinity of individual FA binding sites ($K_A$,$i$), the number $N_L$ of loaded FA equivalents and the absolute distance values $r_{Y,i,j,k}$ themselves. A good estimate for the choice of a relative weight $f_m$ is to take $f_{LS} \approx \langle n \rangle_X - 1$ and $f_{FA} \approx 2 - \langle n \rangle_X$ from spin counting (Figure 4A). The distance values $r_{Y,i,j,k}$ bear an additional complication that is based on the blurred distribution shape and an increased distribution width for long distances above 4–5 nm as a consequence of long-range order and the short achievable dipolar evolution times $t_{max}$ in this experimental setup. The relative fraction of involved interspin distances from each system (here: $N_{LS}/N_{r,LS} = 7/28 = {}^1/_4$) is assumed to have an additional influence on the distribution shape. Therefore, the detailed theoretical prediction of the experimental distance distribution shape is currently considered as largely inaccessible, while individual peak positions are still quite informative.

Nevertheless, the DEER-derived distance distributions of Y-C34R1 XSA allow for an identification of additive features that can be assigned to most of the FAs entering individual binding pockets of XSA.

Finally, another parameter can be used to quantify how $P_{FA}(r)$ dominates the general distribution shape $P(r)$ for higher FA loadings–the first moment of $P(r)$. The first moments, or mean distances $\langle r \rangle$ are typically applied to flexible systems with ambiguous distribution shapes in DEER experiments.[86] Here, $\langle r \rangle_{FA}$ from the corresponding reference distributions 5-XSA $Z_1 0$ (Figure 2B and Figure 5) can be compared with the mean distances $\langle r \rangle$ of individual 5-C34R1 XSA $Z_1 Z_2$ distributions in Figure 3A. The difference in both mean distances of the respective distributions ($\Delta\langle r \rangle = \langle r \rangle - \langle r \rangle_{FA}$) reveal how $P_{FA}(r)$ dominates the general distribution shape for HSA due to its lower labeling efficiency (Figure 6C). The viability of this $\Delta\langle r \rangle$ parameter is thus mainly based on the pertinent large differences ($\Delta\langle r \rangle_{max} > 1$ nm) that emerge for 5-C34R1 HSA with FA loading.

### 2.4 Critical Reflection and Outlook on the Subject

The introduction of a landmark spin bears intrinsic potential for a fundamental strategic advance in understanding the nature of how ligands align in albumin. Distance peaks from bound and spatially largely uncorrelated spin probe ligands in DEER distance distributions[32,38] can be now clearly, but not completely assigned when this topological landmark is introduced to the protein. Here, the feasibility of this approach is provided by combining experimental results from DEER with distances extracted from MD simulations allowing us to perform correlative radial triangulation. The reduced interspin system consisting of only seven LS-$FA_i$ distances ($N_{LS}$) simplifies the standard interspin system ($N_{r,FA} = 21$) that was applied so far for HSA[32] and generally allows for locally tracking bound FAs by DEER when they reside in their individual binding pockets.

The results from 5-C34R1 XSA strongly emphasize that even at low levels of FA loading ($Z_1 Z_2 = 10$) all binding sites are occupied to a certain extent and therefore become traceable, both, with the spin-probing and the with the hybrid spin-probing and spin-labeling approach described here. This means that binding sites $FA_i$ are not filled consecutively, but appear to be rather equally distributed at the applied near-physiological protein/ligand concentrations. The ($FA_i$) distance contributions from the reduced system $P_{LS}(r)$ can be partially identified as singularities ($FA_1$, $FA_2$ and $FA_7$), or are assigned to FA groups as ($FA_2$, $FA_7$) and ($FA_{3\text{-}6}$) in 5-C34R1 XSA and

($FA_4$, $FA_7$) and ($FA_3$, $FA_6$) in 16-C34R1 XSA. To this effect, experimentally inaccessible distances as for $FA_2$ (and $FA_5$) in 16-C34R1 XSA samples (1.5 nm $> r_{Y,i,k} >$ 6.0 nm) also hamper the complete assignment of aligned $Fa_i$ s for now.

Appropriate molecular models and MD simulations have to be used for tracking individual binding sites or groups of them that give clear characteristics in $P(r)$. Once the simulation data are available, any distribution from the system can be reproduced in case all dynamic effects in albumin are quantified that may come along with FA loading. We provide some phenomenological access to this issue and a more precise elaboration on albumins or other systems of overlapping distance distributions upon ligand binding could be studied in future.

The labeling-efficiency ($\varphi_{SH}$) exerts significant influence on the distance distributions $P(r)$ from spin-probed C34R1 XSA, as the desired characteristics LS-FA distances may be clouded by a dominating FA interspin distribution ($P_{FA}(r)$) for higher loadings (see C34R1 HSA in Figure 3 and Figures 5A and 5C). In turn, spin counting in DEER qualitatively confirms the labeling efficiencies that are initially extrapolated from Ellman's tests (e. g., $\varphi_{SH,H,DEER} = \langle n \rangle - 1 = 0.392$ and $\varphi_{SH,H,Ellman} = 0.297$). In combination, this results in the formation of mixture distributions ($P(r)$) that are composed of a superposition from the LS-based ($P_{LS}(r)$) and FA-based ($P_{FA}(r)$) interspin systems (Figures 6A and 6B).

This mixture distribution is expected to occur for albumins with a hypothetical maximum labeling efficiency ($\varphi_{SH} = 1$) as well.

By now, MD simulations still do not fully reproduce $P(r)$ and a more elaborate approach has to be devised to take effects into account like labeling efficiency ($\varphi_{SH}$), individual binding affinities ($K_A$,$i$), just as distance-dependent, analytic and time resolution-related ($t_{max}$) effects,[87] or further conceivable intrinsic restrictions in DEER spectroscopy. Nevertheless, the Tikhonov regularization in combination with DEER data validation that was applied here proved itself as a powerful tool for analyzing these complex DEER time domain data from spin-probed C34R1 XSA, as recurrent characteristics could be identified in $P(r)$ shapes from an independently prepared large number of samples (Figure 3).

One should not exclude the possibility that global allosteric rearrangements occur during FA loading in albumin[73] that may slightly shift expected distance peak positions from theoretical predictions in MD simulations. This claim is also valid for differences in dynamics between HSA and BSA that lead to different ensembles of structures as it was already shown in similar DEER data that were published earlier.[38] In principle, allosteric regulation of albumin by LCFAs is mainly based on shifts in relative orientations of domain I and domain III, relative to domain II.[88,89] This would also explain why $P(r)$ of 5-C34R1 XSA 10 is so broad in the range from 4.5–6.0 nm. In terms of long-range order, we assume this finding represents a multitude of structurally slightly altered FA-loaded states and relative conformational states between these two adjacent domains (I and III). It has to be also concluded that a slightly inhomogeneous ensemble of albumins is captured with DEER, depending on individual loading status ($N_L$), the associated structural rearrangements upon ligand binding, as well as the choice of binding site occupation in each single protein.

Several strategies can be followed to potentially improve our hybrid spin-labeling/spin-probing approach. According to prior studies that aimed for spectral resolution of $^{14}N$ and $^{15}N$ contributions in 2D-DEER on biradicals,[90] or spin-probed polymers using mixed isotopologues for spectral separation (MISS-DEER),[91] a combination of $^{15}N$-MTSSL label and $^{14}N$-DSA ligand could be used in albumin, or vice versa. Currently, the overwhelming number of combinatoric possibilities of potential FA ligand loading experiments still prevents a general straightforward approach to this long standing and elusive albumin issue.

An alternative and simplified approach would be the utilization of a "toolbox" of some established spin-labeled pharmaceuticals (SLPs)[25] or designable phenol-based spin probes[92] that are well-known to represent albumin ligands. Comparative studies on XSA could also provide a quick view on global or local structural effects when the ligand binding sites and their positions are known from crystal structures. So far, all pharmacological ingredients that were investigated by EPR in our group exhibited a decisively lower number of binding sites (e. g. $N_{T,SLP} = 1$–3) and binding affinity values ($K_{A,i} = 2 \cdot 10^2$–$2 \cdot 10^5$ $M^{-1}$)[25] compared to DSA ($N_{T,FA} \approx 8 \pm 1$, $K_A \approx 10^6$–$10^8$ $M^{-1}$).[3,21,23,93] Depending on solubility, a low $K_A$ value is usually accompanied with a high amount of free, or aggregated spectral components (in case of hydrophobic/amphiphilic SLPs in aqueous solution). This, in turn, makes recording meaningful DEER time traces and appropriately analyzing them very tedious, or even impossible. However, first promising achievements have been obtained in the successful application of DEER experiments on some of these pharmacologically relevant ingredients.[94] Note, that by applying these alternative spin probes the maximum number of extended interspin system correlation distances is only $N_{r,LS} = 6$ instead of $N_{r,LS} = 28$ compared to the FA-based system. Of course, this would substantially simplify data evaluation in terms of ligand, or binding site identification.

Recently, a Q-Band DEER study highlighted that the detectable distance range in DEER experiments may be decisively extended to a theoretical value of about 16 nm.[95] This would provide access to the inaccessible distance range from 5–7 nm as seen in the X-Band experiments applied here and maybe even to angular triangulation.[77]

Keeping all these aspects in mind, we are convinced that this proof-of-principle study in combination with the suggested optimization strategies constitutes the onset of a whole series of further conceivable experiments that should complement established $^{13}C$ NMR studies and may contribute to a deeper understanding of the dynamic spatial alignment of fatty acids and other ligands in albumins functional solution structure. Of course, the ultimate goal would be to identify the occupation of individual binding sites only from their DEER-derived

distance characteristics with such an approach. This strategy can be as well expanded to other protein-ligand systems of multivalent binding sites.

## 3. Conclusions

We developed an EPR spectroscopic method that allows for the identification of ligand binding pocket occupations from paramagnetic fatty acids in albumins. The introduction of a covalently attached and thus topologically fixed landmark spin is the first decisive step to disentangle the resulting distance distributions from DEER experiments that are typically of extraordinary complexity. The system is therefore investigated by a combined spin-labeling and spin probing approach.

In a second superordinate step utilizing MD simulations experimental distance characteristics are compared with theoretical distance predictions. Remarkably, most of the systems complexity can be eliminated and we were able to observe mixture distance distributions that are composed from fatty acid-based and landmark spin-based contributions. Essentially, the landmark spin contributions define the straightforward scheme of simultaneous fatty acid, or in general, ligand triangulation strategies in albumins.

Although binding pocket identification cannot be seen as complete by now this approach however offers a new experimental perspective on ligand binding to albumins and proteins in general. In principle each "nameless" ligand is then provided with a characteristic distance and location identity that corresponds to the binding pocket where it may reside. This approach also includes the potential to further investigate such effects as allosteric modulation upon ligand binding, as well as preferential ligand binding site occupation.

## 4. Experimental Section

### 4.1 Materials

Lyophilized powder of HSA (>95%) was obtained from Calbiochem (Merck, Darmstadt, Germany). BSA (>96%), 5-DSA, 16-DSA and phenylhydrazine (97%) were obtained from Sigma Aldrich (St. Louis, MO, USA). The reagents DTT (>99.5%) and dithionitrobenzoic acid (DTNB, >99%) were purchased from AppliChem (Darmstadt, Germany). L-Cysteinechloride monohydrate (>98.5%) and toluene (>99.9%, ROTISOLV HPLC) were obtained from Carl Roth (Karlsruhe, Germany), whereas MTSSL (>98%) was from Enzo Life Sciences (Lörrach, Germany), 87 wt% glycerol from ACROS Organics (Thermo Fisher Scientific, Waltham, MA, USA) and perdeuterated *ortho*-terphenyl (OTP-$d_{14}$, 98 atom % D) from C/D/N Isotopes (Pointe-Claire, Quebec, Canada). Synthesis of the oligoPPE$_1$, oligoPPE$_3$ and oligoPPE/B$_{1\text{-}4}$ dinitroxides (biradicals) was described elsewhere.[65,66] The 0.137 M Dulbecco's phosphate buffered saline (DPBS) pH 7.4 was prepared according to the original procedure[96] and the titration buffers (0.12 M DPBS) for pH adjustment were prepared in the range from pH 0.2–13.5 containing up to 0.6 M hydrochloric acid (HCl) and 0.4 M sodium hydroxide (NaOH).

### 4.2 Spin-Labeling of HSA and BSA

The spin-labeled albumin samples were obtained by incubating 0.2 mM unmodified albumin (XSA, X∈B,H) in 0.136 M DPBS buffer with a 5-fold molar excess of MTSSL and 1% ethanol. 8 ml of this solution was incubated at room temperature in the dark for 16–24 hours at pH 7.3 ± 0.1. The resulting spin-labeled C34R1 XSA samples were separated from the incubation solution with PD-10 columns (Sephadex G-25 resins, GE Healthcare, Chicago, IL, USA). This is because the incubation solution may contain residual unreacted MTSSL monomer and MTSSL dimer.[97–99] Individual fractions were tested with Bradford reagent[100] for qualitative protein content. An additional investigation was conducted utilizing CW EPR spectroscopy to test whether all MTSSL monomers and dimers were removed (Figure S1 and S2). The purified C34R1 XSA solutions were concentrated with spin columns (Sartorius, Göttingen, Germany) and a benchtop centrifuge (Eppendorf Centrifuge 5810 R, Eppendorf AG, Hamburg, Germany) to stock solutions of about 0.3–0.5 ml volume. With the commercially available BCA assay[53] the resulting protein content was determined to be $c_X = 0.42$–$1.53$ mM corresponding to a total yield of up to $\varphi_{prep} = 58\%$ (Pierce™ BCA Protein Assay Kit, Thermo Fisher Scientific).

### 4.3 Ellman's Test

Quantification of accessible thiol groups was conducted with Ellman's reagent (DTNB), according to standard protocols.[52] L-Cysteine was used as a reference to calibrate the strength of the $TNB^{2-}$ color reaction by measuring the characteristic absorption at $\lambda_{Ellman} = 412$ nm[62] on an UV/Vis spectrometer (Hewlett Packard 8453 and 89090 A, HP Inc., Palo Alto, CA, USA). Absorption values and BCA assayed protein concentrations were taken from 1 mM XSA samples of the same lot in order to determine the amount of accessible cysteines per albumin. These labeling efficiency values ($\varphi_{SH,B} = 0.546$ eq R–SH for BSA and $\varphi_{SH,H} = 0.297$ eq R–SH for HSA, see Table 1) can be also used to define the total labeling efficiencies $\varphi_{R1,XSA}$ ($= \varphi_{prep} \cdot \varphi_{SH} = 15$–$33\%$ C34R1 XSA) in the procedure.

### 4.4 MALDI-TOF Mass Spectrometry

Stock solutions of XSA and C34R1 XSA were diluted with ultrapure water (MilliQ) yielding samples with a concentration of 1 mg/ml containing less than 2 mM of salt. MALDI-MS experiments were carried out using a delayed extraction TOF

mass spectrometer Voyager-DE PRO (Sciex, Darmstadt, Germany) equipped with a pulsed nitrogen laser ($\lambda = 337$ nm). Samples were prepared by mixing the sample solutions with the matrix solutions (10 mg/ml sinapinic acid in 0.1% aqueous solution of trifluoroacetic acid/acetonitrile (TFA/ACN), 1:1, v/v) at a ratio of 1:10 (v/v) and 1 µl of the mixture was applied onto a stainless steel sample plate. The sample spots were then dried in a gentle stream of air. Measurements were performed operating in the positive ion linear mode at a total acceleration voltage of 25 kV with a grid voltage set to 92%, 0.15% guide wire voltage and an extraction delay of 700 ns. The low-mass gate was set to *m/z* 10,000 to prevent detector saturation from low mass compounds. The instrument was externally calibrated using BSA and calibration mixture 3 of the Sequazyme Peptide Standards Kit (Sciex). Results are shown in Figure S3–S6.

### 4.5 Preparation of Samples for EPR Spectroscopy

According to the results from Ellman's tests, all C34R1 XSA concentrations were adjusted to $c_{LS} = 0.1$ mM of bound MTSSL, i.e. $c_H = 0.336$ mM for C34R1 HSA and $c_B = 0.183$ mM for C34R1 BSA, assuming $c_X = c_{LS} \cdot \varphi_{SH,X}^{-1}$. This certifies that the SNR in all EPR experiments is good enough for generating DEER time traces of comparable quality and appropriate distance distributions. The stock solutions of paramagnetic fatty acid spin probes (Y-DSA with Y∈5, 16) were prepared with appropriate amounts of 0.1 M potassium hydroxide (KOH) to obtain final stock concentrations of 26 mM. For spin diluted C34R1 XSA samples the reduced and thus largely EPR-silent doxyl stearic acids (26 mM rY-DSA, Figure 1D) were prepared in a slightly modified procedure compared to previous protocols.[32,101] Here, 1 mg of Y-DSA powder was dissolved in 80 µl of 0.1 M KOH to a final concentration of 32.5 mM. These solutions were stirred with gentle agitation. Before each reduction procedure a fresh solution of 66.2 mM phenylhydrazine (PH) was prepared in 0.1 M KOH and mixed thoroughly. 12.5 µl of this PH stock solution was added to 50 µl of 32.5 mM DSA in 0.1 M KOH so that the reaction solution was equipped with 0.5 eq PH and 26 mM Y-DSA. The reaction was allowed to proceed under argon atmosphere at room temperature. Thorough observations of the reduction process were made in the time course of 1.0–1.5 hours (Figure S7) by using a quantitative kinetic approach[102] including double integration routines (Supporting Information S1 and Table S1). The reduction efficiency of both spin probes was about 96–98% after a maximum incubation time of about 40 min.

Appropriate amounts of paramagnetic and diamagnetic spin probes were added as 0.336 mM equivalents for C34R1 HSA and 0.183 mM for C34R1 BSA to yield the desired 0:0, 1:0, 2:0, 1:2, 1:4 and 1:6 loading ratios ($Z_1:Z_2$), whereas each sample then contains one MTSSL, one XSA, $Z_1$ times Y-DSA and $Z_2$ times rY-DSA. As a reference, MTSSL-free XSA samples were prepared at 1:0 and 2:0 loading ratios, again at identical concentrations. The final aqueous solutions of (C34R1) albumins together with the fatty acids were supplied with 20% v/v of glycerol in order to prevent crystallization upon freezing and were titrated to physiological pH 7.40 ± 0.03 and to a volume of 80 µl utilizing appropriate amounts of the aforementioned 0.12 M DPBS titration buffers. Additionally, the effect of 1, 10 and 100 equivalents of DTT on albumin was tested by 24 h incubation with 0.16 mM pure HSA samples that were spin probed with about two 16-DSA ligands (Figure S2A).

The oligoPPE dinitroxides were prepared in the concentration range from 0.27–0.85 mM in OTP-$d_{14}$ (see Figure S8) similar to a procedure described in Godt et al.[65] The yellowish dinitroxide powders (0.1 mg each) were dissolved in 500 µl toluene for transferring them. The toluene volume was then vaporized overnight at room temperature yielding a homogenous laminar layer of evenly spread oligoPPE dinitroxide. About 100–150 mg of OTP-$d_{14}$ was added to the dry dinitroxide and thereafter a heat gun (HL 2010 E electronic, STEINEL Vertrieb GmbH, Herzebrock-Clarholz, Germany) was used for melting the OTP-$d_{14}$ powder (melting point of OTP-$d_{14}$ = 57–59 °C). The hot liquid OTP-$d_{14}$/dinitroxide mixture was then gently stirred for obtaining an even distribution of molecules. The solution was placed on a heater plate at 70–80 °C, ensuring that none of the obtained OTP-$d_{14}$-based liquids solidify and that all air bubbles in the bulk solution have vanished.

In Table S2 more information can be found about the dinitroxides. Finally, an EPR sample tube (Heraeus Quarzglas, inner diameter Ø = 3 mm) was filled with a sterile soda-lime glass Pasteur pipette (Carl Roth, outer diameter Ø = 1.3 mm), again under continuous flow of hot air. For CW EPR experiments about 15 µl of the final protein-containing solutions were filled into micropipettes (BLAUBRAND® IntraMARK, outer diameter Ø = 1.0 mm). For corresponding DEER measurements about 40–80 µl of the solutions were filled into EPR sample tubes and were subsequently shock-frozen in liquid nitrogen-cooled 2-methylbutane for distance measurements.

### 4.6 EPR Spectroscopy

#### *4.6.1 CW EPR Spectroscopy*

A Miniscope MS400 (Magnettech GmbH, Berlin, Germany) benchtop spectrometer was used for X-band CW EPR measurements at microwave frequencies of 9.41–9.43 GHz that was equipped with a frequency counter (RACAL DANA, model 2101, Racal Electronics, Weybridge, UK). All measurements were performed at 25 °C using modulation amplitudes of 0.1 mT and a sweep width of 15 mT (see e.g. Figure 2A and Figure S9).

#### 4.6.2 DEER Spectroscopy

In order to retrieve nanoscale distance information from Y-DSA-probed XSA, C34R1 XSA and the dinitroxides, the four-pulse DEER sequence:[35,36] $\pm(\pi/2)_{obs}$–$\tau_1$–$(\pi)_{obs,1}$–$(t_d+t_0+N_t\cdot\Delta t)$–$(\pi)_{pump}$–$(t'-N_t\cdot\Delta t+t_d)$–$(\pi)_{obs,2}$–$\tau_2$-*echo* was used to obtain dipolar time evolution data. All pulse EPR experiments were performed at X-band frequencies of 9.1–9.4 GHz using a BRUKER Elexsys E580 spectrometer equipped with a BRUKER Flexline splitring resonator ER4118X-MS3 (BRUKER, Billerica, MA, USA). The temperature was set to 50 K for all experiments by cooling with a closed cycle cryostat (ARS AF204, customized for pulse EPR, ARS, Macungie, PA, USA) and the resonator was overcoupled to $Q \approx 200$. The pump frequency $\nu_{pump}$ was set to the maximum of the field swept electron spin echo (ESE)-detected spectrum. The observer frequency $\nu_{obs}$ was set to $\nu_{pump}+\Delta\nu$ with $\Delta\nu$ being in the range of 65 MHz and therefore coinciding with the low field local maximum of the nitroxide ESE spectrum. The observer pulse lengths for each DEER experiment were set to 32 ns for both $\pi/2$- and $\pi$-pulses and the pump pulse length was 12 ns. Additionally, a 2-step phase cycle ($\pm$) was applied to the first $\pi/2$ pulse of the observer frequency for cancelling out receiver offsets and unwanted echoes. Proton modulation was averaged by addition of eight time traces of variable $\tau_1$ starting with $\tau_{1,1}=200$ ns, incrementing by $\Delta\tau_1=8$ ns and ending up at $\tau_{1,8}=256$ ns. For all samples the pump pulse position $t_d+t_0$ after the first observer $\pi$-pulse deadtime $t_d$ was typically incremented for $N_t$ timesteps of $\Delta t=8$ ns in the range $t_0+t'=\tau_1+\tau_2-2t_d$, whereas $\tau_1$ and $\tau_2$ were kept constant. DEER time traces for were recorded for 12–48 hours for spin probed Y-C34R1 XSA giving rise to reliable distance information in between about 1.8 and 5.2 nm as the maximum accessible dipolar evolution times were about $t_{max}\approx 2.3$ µs throughout.[37] All recorded raw time domain DEER data of Y-C34R1 XSA $Z_1Z_2$ are presented in Figures S17–S19.

As the model dinitroxides were embedded in a deuterated matrix (OTP-$d_{14}$) the maximum echo amplitude was found for $\tau_1=396$ ns and $t_{SRT}=3.0$ ms. Dipolar evolution times and time increments were adjusted in the range from $\tau_2=4$–22 µs and $\Delta t=8$–32 ns, respectively. This was done in order to keep the number of data points in the range $400<N_t<700$ and keep the experiment time below about 4 hours. A conventional $^1$H modulation averaging procedure was applied as for DSA-probed HSA as $^2$D modulation from OTP-$d_{14}$ was found to have a minor effect on the distance distributions. Raw time domain DEER data of dinitroxides are presented in Figure S10.

### 4.7 Molecular Models and MD Simulations

All molecular models of 5- and 16-C34R1 HSA 70 were constructed from the structure of HSA co-crystallized with seven stearic acids (PDB ID: 1e7i)[28] using the YASARA Structure software.[83] The implementation of radical-bearing nitroxides ($NO^\bullet$) in MD simulations usually affords special parametrization, but were here modeled as a keto (C=O) groups due to an almost similar bond length.[32,103] As an example the nitroxide bond length for Fremy's salt was found to range about $1.275\pm0.024$ Å.[104]

MD simulations were performed in simulation boxes with periodic cell boundaries containing the protein and an explicit water solvent with 88.300–89.000 atoms in total. The simulation runtime was $t_{MD}=21.3$–27.1 ns at pH 7.4 in 154 mM NaCl and $T=298$ K applying the AMBER03 force-field. All distance trajectories of $r_{Y,i,k}$ are given in Figure S11 ($P_{LS}(r)$). The extracted $8\times8$ distance matrices for 0.0 ns, 3.8 ns and 9.4 ns simulation runtimes $t_{MD}$ of the full interspin system $P(r)$ consisting of all C34R1 and $FA_i$ nitroxide correlations (LS-$FA_i$ distances) are given in Tables S3–S5 and were used to assign $FA_i$ distance peaks, as well as for creating theoretical distance distributions ($Z_1Z_2=70$, see Figure S12) according to a strategy that is explicitly presented in Supporting Information S2. The theoretical distance values of the reduced system $P_{LS}(r)$ in Table 2 were averaged across 10–15 individual values after ca. $t_{MD}>5$–6 ns runtime when all values exhibited relatively constant values. Theoretical distance distributions $P(r)$, $P_{FA}(r)$ and $P_{LS}(r)$ of 5- and 16-C34R1 XSA 70 (Figure 5 and Figure 6) were each constructed from the 9.4 ns simulation snapshot (see also Table S5).

### 4.8 EPR Data Analysis

CW EPR spectra of C34R1 XSA 00 were analyzed in MATLAB 2008b (v.7.7) utilizing the EasySpin software package.[105] This software comprises routines that implement the theory of slow tumbling nitroxides as mainly pioneered by Freed and coworkers.[106,107] Similar to a procedure reported recently[108] all MATLAB codes were optimized for 4-component nitroxide spectra comprising three immobilized components ($b_1$, $b_2$ and $b_3$) and a single free component ($f$). For successful reconstructions of experimental spectra (see Table S6 and Figure S13) starting values for magnetic parameters of MTSSL were taken from Steinhoff et al.[109] Double integration of CW EPR spectra $S(B)$ of C34R1 XSA 00 with 0.1 mM MTSSL confirmed the validity of this approach with an error of only about 10% compared to the average value ($DI=\iint S(B)d^2B=(5.28\pm0.53)\cdot10^5$).

A second moment analysis[110] was performed on C34R1 XSA 00 according to standard procedures in CW EPR spectroscopy[111,112] that allow for mapping the dynamic protein topology surrounding the spin label.[113–115] Further details about such EPR-analytic technicalities in this regard can be found in Supporting Information S3.

All collected DEER time traces have been analyzed in a consistent manual fit procedure with DeerAnalysis2013 utilizing Tikhonov regularization.[67] The regularization parameters were set to $\alpha_{16}=100$ and $\alpha_5=1000$ for Y-C34R1 XSA $Z_1Z_2$ and Y-XSA $Z_1Z_2$ samples for all datasets in order to obtain comparable distance peak resolutions. All time trace back-

ground dimensionalities have been set to $D = 3.74 \pm 0.03$, apart from the C34R1 XSA 00 samples where $D = 2.94$–$2.96$ suited best to reproduce the largely modulation-free DEER time traces (*monoradical* albumins). The raw data of spin-probed unmodified XSA can be found in Figure S14. Validated DEER data from corresponding samples were obtained throughout by varying background dimensionalities ($D$) and background correction starting times. The experimental distributions $P(r)$ are reliable up to about 4.5–5.0 nm. Additional raw DEER data ($V(t)/V(0)$) are presented together with the validation results in Figures S17–S19.

DEER time traces of dinitroxides were analyzed with fitted background dimensionalities ranging from $3.17 < D < 3.55$. The distance-independent value of the modulation depth parameter of the E580 pulse EPR machine equipped with the Flexline splitring resonator ER4118X-MS3 was determined as $\lambda = 0.534 \pm 0.009$ (Figure S15) similar to an approach already outlined by Hilger et al.[68] This value can be used for spin counting procedures on all Y-C34R1 XSA $Z_1Z_2$ samples (see Supporting information S4), where the number of coupled spins $\langle n \rangle$ residing in an isolated EPR-active cluster is just given as:[67]

$$\langle n \rangle = 1 - \frac{\ln(1 - \Delta)}{\lambda} \tag{3}$$

in a first approximation. A complete set of dipolar evolution functions $F(t)/F(0)$ with regularized fit curves and DEER distance distributions $P(r)$ of all experiments on Y-C34R1 XSA $Z_1Z_2$ can be found in Figure 3. The differences in first moments ($\Delta\langle r \rangle$) from distance distributions of 5-C34R1 XSA and corresponding reference data (5-XSA) were determined from corresponding DeerAnalysis2013 output-files as a qualitative measure for peak shifts in $P(r)$ (see Figure 6C). Modulation depth raw data from Y-C34R1 XSA $Z_1Z_2$ samples are presented in Figure S16 and can be converted to $\langle n \rangle$ with equation 3.

## Acknowledgements

The authors thank Heike Schimm and Stefanie Weber for technical support. We gratefully acknowledge financial support from the Fraunhofer Internal Program under Grant No. Attract 069-608203 (C. E. H. S.) and from the Deutsche Forschungsgemeinschaft (DFG) under grant number HI 1094/5-1 and SFB TRR 102. Useful hints regarding the MD simulations were kindly given by Dr. Felix Hoffmann, Martin Luther University Halle-Wittenberg, Germany. Additionally, we are grateful to Prof. Dr. Gunnar Jeschke, ETH Zürich, Switzerland for helpful discussions on the DEER experiments on oligoPPE dinitroxides.

## References

[1] T. Peters Jr., *All about albumin: biochemistry, genetics, and medical applications*, Academic Press, San Diego, CA, **1996**.
[2] A. A. Spector, K. John, J. E. Fletcher, *J. Lipid Res.* **1969**, *10*, 56–67.
[3] T. G. Gantchev, M. B. Shopova, *Biochim. Biophys. Acta Protein Struct. Mol. Enzymol.* **1990**, *1037*, 422–434.
[4] E. S. Krenzel, Z. Chen, J. A. Hamilton, *Biochemistry* **2013**, *52*, 1559–1567.
[5] C. Tanford, *Physical chemistry of macromolecules*, John Wiley & Sons, Inc., New York, NY, **1961**, pp. 526–586.
[6] J. E. Fletcher, A. A. Spector, J. D. Ashbrook, *Biochemistry* **1970**, *9*, 4580–4587.
[7] J. E. Fletcher, J. D. Ashbrook, A. A. Spector, *Ann. N. Y. Acad. Sci.* **1973**, *226*, 69–81.
[8] D. S. Goodman, *J. Am. Chem. Soc.* **1958**, *80*, 3892–3898.
[9] A. A. Spector, J. E. Fletcher, J. D. Ashbrook, *Biochemistry* **1971**, *10*, 3229–3232.
[10] J. D. Ashbrook, A. A. Spector, E. C. Santos, J. E. Fletcher, *J. Biol. Chem.* **1975**, *250*, 2333–2338.
[11] A. A. Spector, *J. Lipid Res.* **1975**, *16*, 165–179.
[12] J. A. Hamilton, D. P. Cistola, J. D. Morrisett, J. T. Sparrow, D. M. Small, *Proc. Natl. Acad. Sci. USA* **1984**, *81*, 3718–3722.
[13] T. Oida, *J. Biochem.* **1986**, *100*, 1533–1542.
[14] D. P. Cistola, D. M. Small, J. A. Hamilton, *J. Biol. Chem.* **1987**, *262*, 10971–10979.
[15] D. P. Cistola, D. M. Small, J. A. Hamilton, *J. Biol. Chem.* **1987**, *262*, 10980–10985.
[16] D. P. Cistola, D. M. Small, *J. Clin. Invest.* **1991**, *87*, 1431–1441.
[17] J. A. Hamilton, S. Era, S. P. Bhamidipati, R. G. Reed, *Proc. Natl. Acad. Sci. USA* **1991**, *88*, 2051–2054.
[18] R. W. Sarver, H. Gao, F. Tian, *Anal. Biochem.* **2005**, *347*, 297–302.
[19] J. D. Morrisett, H. J. Pownall, A. M. Gotto, Jr., *J. Biol. Chem.* **1975**, *250*, 2487–2494.
[20] H. H. Ruf, M. Gratzl, *Biochim. Biophys. Acta* **1976**, *446*, 134–142.
[21] S. J. Rehfeld, D. J. Eatough, W. Z. Plachy, *J. Lipid Res.* **1978**, *19*, 841–849.
[22] C. B. Berde, B. S. Hudson, R. D. Simoni, L. A. Sklar, *J. Biol. Chem.* **1979**, *254*, 391–400.
[23] R. C. Perkins, Jr., N. Abumrad, K. Balasubramanian, L. R. Dalton, A. H. Beth, J. H. Park, C. R. Park, *Biochemistry* **1982**, *21*, 4059–4064.
[24] J. A. Hamilton, *Biochim. Biophys. Acta Gen. Subj.* **2013**, *1830*, 5418–5426.
[25] T. Hauenschild, J. Reichenwallner, V. Enkelmann, D. Hinderberger, *Chem. Eur. J.* **2016**, *22*, 12825–12838.
[26] S. Curry, H. Mandelkow, P. Brick, N. Franks, *Nat. Struct. Biol.* **1998**, *5*, 827–835.
[27] S. Curry, P. Brick, N. P. Franks, *Biochim. Biophys. Acta Mol. Cell Biol. Lipids* **1999**, *1441*, 131–140.
[28] A. A. Bhattacharya, T. Grüne, S. Curry, *J. Mol. Biol.* **2000**, *303*, 721–732.
[29] J. R. Simard, P. A. Zunszain, C. E. Ha, J. S. Yang, N. V. Bhagavan, I. Petitpas, S. Curry, J. A. Hamilton, *Proc. Natl. Acad. Sci. USA* **2005**, *102*, 17958–17963.
[30] J. R. Simard, P. A. Zunszain, J. A. Hamilton, S. Curry, *J. Mol. Biol.* **2006**, *361*, 336–351.
[31] J. Reichenwallner, D. Hinderberger, *Biochim. Biophys. Acta Gen. Subj.* **2013**, *1830*, 5382–5393.

[32] M. J. N. Junk, H. W. Spiess, D. Hinderberger, *Angew. Chem. Int. Ed.* **2010**, *49*, 8755–8759.
[33] M. J. N. Junk, H. W. Spiess, D. Hinderberger, *J. Magn. Reson.* **2011**, *210*, 210–217.
[34] M. J. N. Junk, H. W. Spiess, D. Hinderberger, *Biophys. J.* **2011**, *100*, 2293–2301.
[35] R. E. Martin, M. Pannier, F. Diederich, V. Gramlich, M. Hubrich, H. W. Spiess, *Angew. Chem. Int. Ed.* **1998**, *37*, 2834–2837.
[36] M. Pannier, S. Veit, A. Godt, G. Jeschke, H. W. Spiess, *J. Magn. Reson.* **2000**, *142*, 331–340.
[37] G. Jeschke, *Annu. Rev. Phys. Chem.* **2012**, *63*, 419–446.
[38] Y. Akdogan, J. Reichenwallner, D. Hinderberger, *PLoS One* **2012**, *7*, e45681.
[39] S. S. Eaton, G. R. Eaton, *Coord. Chem. Rev.* **1978**, *26*, 207–262.
[40] A. V. Kulikov, G. I. Likhtenstein, *Adv. Mol. Relax. Interact. Processes* **1977**, *10*, 47–79.
[41] B. Joseph, A. Sikora, E. Bordignon, G. Jeschke, D. S. Cafiso, T. F. Prisner, *Angew. Chem.* **2015**, *127*, 6294–6297.
[42] B. Joseph, V. M. Tormyshev, O. Y. Rogozhnikova, D. Akhmetzyanov, E. G. Bagryanskaya, T. F. Prisner, *Angew. Chem. Int. Ed.* **2016**, *55*, 11538–11542.
[43] T. J. Stone, T. Buckman, P. L. Nordio, H. M. McConnell, *Proc. Natl. Acad. Sci. USA* **1965**, *54*, 1010–1017.
[44] O. H. Griffith, H. M. McConnell, *Proc. Natl. Acad. Sci. USA* **1966**, *55*, 8–11.
[45] J. Reichenwallner, M. T. Oehmichen, C. E. H. Schmelzer, T. Hauenschild, A. Kerth, D. Hinderberger, *Magnetochemistry* **2018**, *4*, 47.
[46] D. S. Park, C. E. Petersen, C. E. Ha, K. Harohalli, J. B. Feix, and N. V. Baghavan, *IUBMB Life* **1999**, *48*, 169–174.
[47] T. Hauenschild, Diploma thesis, Johannes Gutenberg-Universität Mainz, Germany, **2013**.
[48] Y. Shenberger, A. Shimshi, S. Ruthstein, *J. Phys. Chem. B* **2015**, *119*, 4824–4830.
[49] C. M. Gruian, C. Rickert, S. C. T. Nicklisch, E. Vanea, H. J. Steinhoff, S. Simon, *ChemPhysChem* **2017**, *18*, 634–642.
[50] S. Sugio, A. Kashima, S. Mochizuki, M. Noda, K. Kobayashi, *Protein Eng.* **1999**, *12*, 439–446.
[51] K. A. Majorek, P. J. Porebski, A. Dayal, M. D. Zimmerman, K. Jablonska, A. J. Stewart, M. Chruszcz, W. Minor, *Mol. Immunol.* **2012**, *52*, 174–182.
[52] G. L. Ellman, *Arch. Biochem. Biophys.* **1959**, *82*, 70–77.
[53] P. K. Smith, R. I. Krohn, G. T. Hermanson, A. K. Mallia, F. H. Gartner, M. D. Provenzano, E. K. Fujimoto, N. M. Goeke, B. J. Olson, D. C. Klenk, *Anal. Biochem.* **1985**, *150*, 76–85.
[54] L. J. Berliner, J. Grunwald, H. O. Hankovszky, K. Hideg, *Anal. Biochem.* **1982**, *119*, 450–455.
[55] J. B. Feix, C. S. Klug, in *Spin Labeling: The Next Millenium*, Vol. 14 (Ed.: L. J. Berliner), Kluwer Academic Publishers, New York, NY, **2002**, pp. 251–281.
[56] J. Janatova, J. K. Fuller, M. J. Hunter, *J. Biol. Chem.* **1968**, *243*, 3612–3622.
[57] K. Oettl, R. E. Stauber, *Br. J. Pharmacol.* **2007**, *151*, 580–590.
[58] K. Oettl, G. Marsche, *Methods Enzymol.* **2010**, *474*, 181–195.
[59] M. Anraku, V. T. G. Chuang, T. Maruyama, M. Otagiri, *Biochim. Biophys. Acta Gen. Subj.* **2013**, *1830*, 5465–5472.
[60] J. Bonanata, L. Turell, L. Antmann, G. Ferrer-Sueta, S. Botasini, E. Mendez, B. Alvarez, E. L. Coitino, *Free Radical Biol. Med.* **2017**, *108*, 952–962.
[61] I. D. Pavicevic, V. B. Jovanovic, M. M. Takic, A. Z. Penezic, J. M. Acimovic, L. M. Mandic, *Chem.-Biol. Interact.* **2014**, *224*, 42–50.
[62] C. K. Riener, G. Kada, H. J. Gruber, *Anal. Bioanal. Chem.* **2002**, *373*, 266–276.
[63] G. Jeschke, M. Sajid, M. Schulte, A. Godt, *Phys. Chem. Chem. Phys.* **2009**, *11*, 6580–6591.
[64] A. Godt, C. Franzen, S. Veit, V. Enkelmann, M. Pannier, G. Jeschke, *J. Org. Chem.* **2000**, *65*, 7575–7582.
[65] A. Godt, M. Schulte, H. Zimmermann, G. Jeschke, *Angew. Chem.* **2006**, *118*, 7722–7726.
[66] G. Jeschke, M. Sajid, M. Schulte, N. Ramezanian, A. Volkov, H. Zimmermann, A. Godt, *J. Am. Chem. Soc.* **2010**, *132*, 10107–10117.
[67] G. Jeschke, V. Chechik, P. Ionita, A. Godt, H. Zimmermann, J. Banham, C. R. Timmel, D. Hilger, H. Jung, *Appl. Magn. Reson.* **2006**, *30*, 473–498.
[68] D. Hilger, H. Jung, E. Padan, C. Wegener, K. P. Vogel, H. J. Steinhoff, G. Jeschke, *Biophys. J.* **2005**, *89*, 1328–1338.
[69] A. D. Milov, A. B. Ponomarev, Y. D. Tsvetkov, *Chem. Phys. Lett.* **1984**, *110*, 67–72.
[70] B. E. Bode, D. Margraf, J. Plackmeyer, G. Dürner, T. F. Prisner, O. Schiemann, *J. Am. Chem. Soc.* **2007**, *129*, 6736–6745.
[71] D. R. Kattnig, J. Reichenwallner, D. Hinderberger, *J. Phys. Chem. B* **2013**, *117*, 16542–16557.
[72] C. Tanford, J. G. Buzzell, *J. Phys. Chem.* **1956**, *60*, 225–231.
[73] N. Ahalawat, R. K. Murarka, *J. Biomol. Struct. Dyn.* **2015**, *33*, 2192–2204.
[74] J. Ghuman, P. A. Zunszain, I. Petitpas, A. A. Bhattacharya, M. Otagiri, S. Curry, *J. Mol. Biol.* **2005**, *353*, 38–52.
[75] M. A. Kiselev, I. A. Gryzunov, G. E. Dobretsov, M. N. Komarova, *Biofizika* **2001**, *46*, 423–427.
[76] J. E. Lovett, A. M. Bowen, C. R. Timmel, M. W. Jones, J. R. Dilworth, D. Caprotti, S. G. Bell, L. L. Wong, J. Harmer, *Phys. Chem. Chem. Phys.* **2009**, *11*, 6840–6848.
[77] A. Savitsky, A. A. Dubinskii, H. Zimmermann, W. Lubitz, K. Möbius, *J. Phys. Chem. B* **2011**, *115*, 11950–11963.
[78] A. Marko, T. F. Prisner, *Phys. Chem. Chem. Phys.* **2013**, *15*, 619–627.
[79] I. Tkach, S. Pornsuwan, C. Hobärtner, F. Wachowius, S. T. Sigurdsson, T. Y. Baranova, U. Diederichsen, G. Sicoli, M. Bennati, *Phys. Chem. Chem. Phys.* **2013**, *15*, 3433–3437.
[80] F. Karush, *J. Am. Chem. Soc.* **1950**, *72*, 2705–2713.
[81] F. Karush, *J. Am. Chem. Soc.* **1954**, *76*, 5536–5542.
[82] J. Reichenwallner, A. Thomas, T. Steinbach, J. Eisermann, C. E. H. Schmelzer, F. Wurm, D. Hinderberger, *Biomacromolecules* **2019**, *20*, 1118–1131.
[83] E. Krieger, G. Koraimann, G. Vriend, *Proteins Struct. Funct. Genet.* **2002**, *47*, 393–402.
[84] R. A. Redner, H. F. Walker, *SIAM Rev.* **1984**, *26*, 195–239.
[85] J. G. Morel, N. K. Nagaraj, *Biometrika* **1993**, *80*, 363–371.
[86] G. Jeschke, G. Panek, A. Godt, A. Bender, H. Paulsen, *Appl. Magn. Reson.* **2004**, *26*, 223–244.
[87] G. Jeschke, A. Koch, U. Jonas, A. Godt, *J. Magn. Reson.* **2002**, *155*, 72–82.
[88] S. Curry, *Vox Sang.* **2002**, *83*, 315–319.
[89] M. Fasano, S. Curry, E. Terreno, M. Galliano, G. Fanali, P. Narciso, S. Notari, P. Ascenzi, *IUBMB Life* **2005**, *57*, 787–796.
[90] G. Jeschke, H. Zimmermann, A. Godt, *J. Magn. Reson.* **2006**, *180*, 137–146.
[91] D. Kurzbach, D. R. Kattnig, B. Zhang, A. D. Schlüter, D. Hinderberger, *Chem. Sci.* **2012**, *3*, 2550–2558.
[92] T. Hauenschild, D. Hinderberger, *ChemPlusChem* **2019**, *84*, 43–51.
[93] J. Reichenwallner, PhD thesis, Martin Luther University Halle-Wittenberg, **2018**.

[94] T. Hauenschild, PhD thesis, Martin Luther University Halle-Wittenberg, **2018**.
[95] T. Schmidt, M. A. Wälti, J. L. Baber, E. J. Hustedt, G. M. Clore, *Angew. Chem. Int. Ed.* **2016**, *55*, 15905–15909.
[96] R. Dulbecco, M. Vogt, *J. Exp. Med.* **1954**, *99*, 167–182.
[97] V. V. Khramtsov, L. B. Volodarsky, in *Spin Labeling: The Next Millenium,* Vol. 14 (Ed.: L. J. Berliner), Kluwer Academic Publishers, New York, NY, **2002**, pp. 109–180.
[98] V. V. Khramtsov, I. A. Grigor'ev, M. A. Foster, D. J. Lurie, *Antioxid. Redox Signaling* **2004**, *6*, 667–676.
[99] S. Bleicken, A. J. Garcia-Saez, E. Conte, E. Bordignon, *PLoS One* **2012**, *7*, e35910.
[100] M. M. Bradford, *Anal. Biochem.* **1976**, *72*, 248–254.
[101] T. D. Lee, J. F. W. Keana, *J. Org. Chem.* **1975**, *40*, 3145–3147.
[102] A. A. Pavicevic, A. D. Popovic-Bijelic, M. D. Mojovic, S. V. Susnjar, G. G. Bacic, *J. Phys. Chem. B* **2014**, *118*, 10898–10905.
[103] F. H. Allen, O. Kennard, D. G. Watson, L. Brammer, A. G. Orpen, R. Taylor, *J. Chem. Soc. Perkin Trans. 2* **1987**, S1–S19.
[104] H. Elgabarty, M. Wolff, A. Glaubitz, D. Hinderberger, D. Sebastiani, *Phys. Chem. Chem. Phys.* **2013**, *15*, 16082–16089.
[105] S. Stoll, A. Schweiger, *J. Magn. Reson.* **2006**, *178*, 42–55.
[106] J. H. Freed, in *Spin Labeling: Theory and Applications*, Vol. 1 (Ed.: L. J. Berliner), Academic Press, New York, NY, **1976**, pp. 53–132.
[107] D. J. Schneider, J. H. Freed, in *Spin Labeling: Theory and Applications*, Vol. 8 (Eds.: L. J. Berliner, J. Reuben), Plenum Press, New York, NY, **1989**, pp. 1–76.
[108] J. Reichenwallner, A. Thomas, L. Nuhn, T. Johann, A. Meister, H. Frey, D. Hinderberger, *Polym. Chem.* **2016**, *7*, 5783–5798.
[109] H. J. Steinhoff, W. L. Hubbell, *Biophys. J.* **1996**, *71*, 2201–2212.
[110] C. Benoit, E. Royer, G. Poussigue, *J. Phys. Condens. Matter* **1992**, *4*, 3125–3152.
[111] W. L. Hubbell, C. Altenbach, *Curr. Opin. Struct. Biol.* **1994**, *4*, 566–573.
[112] E. Bordignon, H. J. Steinhoff, in *ESR spectroscopy in membrane biophysics*, Vol. 27 (Eds.: M. A. Hemminga, L. J. Berliner), Springer Science + Business Media, LLC, New York, NY, **2007**, pp. 129–164.
[113] W. L. Hubbell, H. S. Mchaourab, C. Altenbach, M. A. Lietzow, *Structure* **1996**, *4*, 779–783.
[114] H. S. Mchaourab, M. A. Lietzow, K. Hideg, W. L. Hubbell, *Biochemistry* **1996**, *35*, 7692–7704.
[115] J. M. Isas, R. Langen, H. T. Haigler, W. L. Hubbell, *Biochemistry* **2002**, *41*, 1464–1473.

Manuscript received: June 25, 2019
Revised manuscript received: November 10, 2019
Version of record online: November 18, 2019

  